

Paramagnetic point defects in (100)Si/LaAlO₃ structures: Nature and stability of the interface

K. Clémer, A. Stesmans,^{a)} and V. V. Afanas'ev

Department of Physics, University of Leuven, 3001 Leuven, Belgium and Institute for Nanoscale Physics and Chemistry (INPAC), University of Leuven, Belgium

L. F. Edge and D. G. Schlom

Department of Materials Science and Engineering, Pennsylvania State University, University Park, Pennsylvania 16802

(Received 8 February 2007; accepted 14 May 2007; published online 15 August 2007)

The atomic nature of the interface in (100)Si/LaAlO₃ structures with nanometer-thin amorphous LaAlO₃ layers of high dielectric constant (κ), deposited directly on clean (100)Si by molecular beam deposition at ~ 100 °C, was assessed through probing of paramagnetic point defects. On the as-grown samples *K*-band electron spin resonance indicated the absence of a Si/SiO₂-type interface in terms of the archetypal Si-dangling bond-type Si/SiO₂ interface defects (P_{b0} , P_{b1}). With no P_b -type defects observed, this state is found to persist during subsequent annealing (1 atm N₂ or 5% O₂ in N₂ ambient) up to the temperature $T_{\text{an}} \sim 800$ °C, referring to a thermally stable abrupt Si/LaAlO₃ interface, quite in contrast with other high- κ metal oxide/Si structures. However, in the range $T_{\text{an}} \sim 800$ – 860 °C a Si/SiO₂-type interface starts forming as evidenced by the appearance of P_{b0} defects and, with some delay in T_{an} , the EX center—a SiO₂ associated defect, attesting to significant structural/compositional modification. The peaking of the defect density versus T_{an} curves indicates the SiO_x nature of the interlayer to break up again upon annealing at $T_{\text{an}} \geq 930$ °C, possibly related to crystallization and/or degrading silicate formation. No specific LaAlO₃-specific point defects could be traced. © 2007 American Institute of Physics.
[DOI: [10.1063/1.2749423](https://doi.org/10.1063/1.2749423)]

I. INTRODUCTION

The relentless scaling in integrated circuit (IC) technology based on the silicon complementary metal oxide semiconductor (CMOS) concept has driven IC technology to a historical move.^{1,2} The progress requires the replacement of the classical SiO₂ (SiON) gate dielectric by an insulator of significantly higher dielectric constant κ than that of SiO₂ [$\kappa(\text{SiO}_2) \cong 3.9$]³—the high- κ issue—which, since its conception, has ensued a vivid activity in current applied semiconductor research. The use of these high- κ dielectrics would allow the application of physically thicker films of equivalent SiO₂ electrical (capacitive) oxide thickness (EOT) required to be reduced to less than 1 nm for future realization of MOS gate lengths < 30 nm.³

For that purpose, a large variety of (metal) oxides have been investigated as possible candidates, including metal oxides in their simplest form such as HfO₂, ZrO₂, Al₂O₃, La₂O₃, and others,^{1,4} as well as more complex varieties such as silicates, aluminates, pseudobinary mixtures, and multivalent metal oxide compounds. Presently, HfO₂, or better stated, the HfO₂-based composites (e.g., HfO_xSi_yN_z), have emerged as the most promising future gate oxides.^{3,5}

Obviously, the replacing high- κ insulator must meet various stringent requirements, such as exhibiting thermodynamic stability in contact with Si, a band gap over 5 eV, sufficient band offsets with silicon, and a low interface trap

density.² Eventually, apart from the higher κ value, it should approach the superb performance of the SiO₂ layer on Si. Perhaps, most crucially, like the Si/SiO₂ system, it should form a technological grade interface with Si, simultaneously combining high abruptness to enable the realization of small EOTs. The interfacial electrical properties should be close to, or if possible, even supersede those of the standard Si/SiO₂ interface. Moreover, the interface should be able to endure the various thermal steps required for device processing.

Typically, however, with high- κ metal oxide layers on Si, already in the as-deposited state or after required thermal steps, a SiO_{2(x)} interlayer forms, making the interface Si/SiO_{2(x)}-like. The presence of such an interlayer has been revealed by numerous topographic/imaging techniques, such as medium-energy ion scattering (MEIS), high-resolution transmission electron microscopy (HRTEM), and x-ray photoelectron spectroscopy (XPS).^{1,4,6–13} On atomic scale this Si/SiO_{2(x)}-like interface nature has early on been demonstrated by the observation by electron spin resonance (ESR) of the typical P_b -type interface centers (*vide infra*), i.e., P_{b0} and P_{b1} —first in stacks of (100)Si with nanometer-thick layers of ZrO₂ and Al₂O₃ grown by the atomic layer chemical vapor deposition (ALCVD) method,¹⁴ and later in (111)Si/HfO₂ with the HfO₂ film grown by ALCVD (Ref. 15) and various (100)Si/HfO₂ entities prepared by CVD.¹⁶ It has since been affirmed by independent analysis.^{17–19} Thus, these results would indicate that the formation of an SiO_{2(x)} interlayer appears endemic for Si/high- κ metal oxide systems. Both by independent electrical measurements^{20–23} and

^{a)}Electronic mail: andre.stesmans@fys.kuleuven.be

ESR observations,^{14,16} it has been evidenced that in this way an interface of technological quality is realized in terms of interface state density^{24–26} and passivation behavior in hydrogen,^{25,27,28} much alike the standard thermal Si/SiO₂ system. While highly beneficial in this respect, it obviously conflicts with the EOT restriction, the more so with increasing relative thickness of the “low- κ ” SiO₂ interlayer. Yet, the insertion of a well (in thickness) controlled SiO₂ layer of minimal thickness is currently adopted as a *modus vivendi* route of progress.^{2,4,29}

II. SI/SiO₂ SPECIFIC DEFECTS

The main body of this work deals with the observation and monitoring of two major types of Si/SiO₂-specific point defects. For the sake of comprehensibility and to later ease discussion, it might be useful to briefly summarize the basic properties of these two distinct types of defects.

A. P_b -type interface defects

Three Si-dangling-bond (DB)-type Si/SiO₂ interface defects have so far been substantiated by ESR, commonly denoted as the P_b -type defects. It has been demonstrated in conjunction with electrical measurements that these P_b -type defects are the dominant class of interface traps (see, e.g., Refs. 30 and 31 for an overview) invariably introduced at the Si/SiO₂ interface as a result of lattice mismatch.^{31–33} The P_b -type defects have not only been observed in Si/SiO₂ entities but, as recalled above, also appear generally inevitable in Si/high- κ structures. There, the uniqueness of the presence of P_b -type defects was taken as convincing evidence for the presence of a SiO_{2(x)}-type interlayer, i.e., a SiO_{2(x)}-type interface. The different types of Si DB-type defects observed correlate with interface orientation, in registry with the crystallinity of the underlying Si substrate. At the (111)Si/SiO₂ interface, the only type observed—specifically termed P_b —was identified as trivalent interfacial Si ($\text{Si}_3 \equiv \text{Si}^\cdot$, where the dot represents an unpaired electron in a dangling Si sp^3 hybrid) backbonded to three Si atoms in the bulk. The technologically favored (100)Si/SiO₂ interface exhibits two types, termed P_{b0} and P_{b1} . The experimental evidence is that P_{b0} is chemically identical to P_b , but now residing at microscopically (100)-oriented Si/SiO₂ facets. In compliance, both were conclusively established as major systems of detrimental electrical interface traps. The P_{b1} center is assigned to a distorted defected interfacial Si–Si dimer ($a \equiv \text{Si}^\cdot\text{--}\text{Si}^\cdot = \text{Si}_2$ defect, where the endash symbolizes a strained bond, with an approximately $\langle 211 \rangle$ oriented unpaired Si sp^3 hybrid).³⁴ At the (110)Si/SiO₂ interface also, only one type, the P_b variant, is observed.^{31,35} Thus all three variants were shown to be interfacial trivalent Si centers,^{32,34,36} naturally occurring, for standard oxidation temperatures (800–960 °C), in areal densities of $[P_b] \sim 5 \times 10^{12} \text{ cm}^{-2}$ (Refs. 30, 33, 36, and 37) and $[P_{b0}], [P_{b1}] \sim 1 \times 10^{12} \text{ cm}^{-2}$.³⁰

B. The EX defect

Another defect of interest for the current work is EX : A SiO₂-associated defect generally observed in Si/SiO₂ entities

after thermal treatment. The EX center was first reported³⁸ for as-prepared SiO₂ thermally grown on (111)Si in dry O₂ at 700–850 °C. Using K -band ESR at low temperatures a narrow isotropic signal was observed with a g value of $g = 2.002\,46 \pm 0.000\,03$ and linewidth $\Delta B_{p,p} = 1.0 \pm 0.05 \text{ G}$ together with a ²⁹Si hyperfine doublet of splitting $a = 16.1 \pm 0.1 \text{ G}$. Later Stesmans and Scheerlinck³⁹ reported the observation of EX in *dry thermal* SiO₂ in (001) and (111)Si/SiO₂ entities. From this study it was shown that the EX areal defect density depends on the grown oxide thickness (d_{ox}), that EX is only detected from $d_{\text{ox}} \sim 70 \text{ \AA}$ onward with a maximum density at $d_{\text{ox}} \sim 125 \text{ \AA}$ and is mainly located in the top 45 Å of the oxide layer. The detection of part of the ¹⁷O hyperfine structures of EX in ¹⁷O enriched (111)Si/SiO₂ structures⁴⁰ resulted in the suggestion of a preliminary model where EX consists of a hole delocalized over four oxygen DBs formally at the site of a Si vacancy. In another view, it has been described as an agglomerate of four oxygen-related hole centers (OHCs).⁴¹

Over the years EX has been observed in a variety of Si/SiO₂ entities and SiO₂ samples such as oxidized porous Si layers,^{41,42} thermally degraded Si/SiO₂,⁴³ silicon nanowires,^{44,45} ultrafine silicon particles,⁴⁶ fumed silica nanoparticles,⁴⁷ and in stacks of nanometer-thick layers of SiO_x, Al₂O₃, ZrO₂, and HfO₂ on (100)Si.^{16,48,49} Dohi *et al.* suggested the presence of two different variants in ultrafine Si particles,⁴⁶ exhibiting the same g value but a different saturation behavior which they labeled EX_L and EX_H . This work further suggested that the EX_H center observed upon annealing of the particles in vacuum at 900–1000 °C is similar to the EX center described above, and that the EX_L center observed upon annealing at 600–700 °C is identical to the defect reported by Kusumoto and Shoji⁵⁰ in Si powders crushed in room ambient which Dohi *et al.* suggest to be related to the Si–OH structure. Most importantly for the current work is that EX is systematically observed in Si/high- κ entities^{16,48,49} and was taken as conclusive evidence for an additional growth or modification of the SiO_x interlayer (IL).

The latter inference, in particular, with respect to the mentioning of additional IL growth, might at first sight appear at odds with the above mentioned result for the standard thermal Si/SiO₂ case, where the EX ESR signal could only be detected from $d_{\text{ox}} \sim 7 \text{ nm}$ onward in (100) Si/SiO₂, as the SiO_x-type IL in Si/high- κ insulator systems is typically in the sub-2 nm range. But here it should be recalled that for the thermal Si/SiO₂ case, the EX appears in the course of open thermal oxidation of a c -Si face, which situation is quite different from the confined and chemically altered IL formation environment in a typical Si/high- κ insulator structure. Should the advanced EX model (i.e., agglomerate of OHCs; formal Si vacancy) basically be correct, the formation of OHCs in such environment is likely to be drastically affected in (potentially) various ways, such as different strain environment, O₂ supply, and the influence of the high- κ layer on top, e.g., in terms of affecting the IL stoichiometry (e.g., Si depletion). Hence, the particular stoichiometric/structural nature of the formed IL—invariably cautiously referred to as SiO_x-type rather than plain SiO₂—may be of such nature so as to promote EX formation to higher local densities than

encountered in standard Si/SiO₂, enabling ESR detection from thinner layers. The interlayers concerned here differ from thermal oxide. In this respect also, as clearly mentioned before, the fact that the *EX* could only be detected by ESR from the thermal oxide thickness $d_{\text{ox}} \sim 7$ nm onward does not necessarily imply the *EX* center not to occur for $d_{\text{ox}} < 7$ nm. It may just mean the total density to remain below the ESR detection limit of $\sim 1 \times 10^{10} \text{ cm}^{-2}$ for such centers. In summary, the confined and chemically altered environment may enhance *EX* defect formation. Conversely, that apparently happening enhancement (see observed defect densities) as indicated by the detectable appearance of *EX* in such thin layers may just be taken as evidence for this. Finally, it is added that the doubt cast⁴⁸ on the previously reported *K*-band detection of the *EX* center in stacks of ultrathin layers of SiO_x, Al₂O₃, ZrO₂, and HfO₂ on (100)Si (Ref. 16) disregards spectroscopic evidence.

III. THE (100)Si/LaAlO₃ STRUCTURE

The presence of an interfacial SiO_x layer in Si/high- κ structures, even though possibly providing the scope of realizing standard Si/SiO₂ interface quality, is not desirable because of the adverse impact on the net EOT. Thus, optimization of EOT would mandate to look for a Si/high- κ insulator system without such a SiO_x interlayer. And of course, it is hoped that this can be achieved hand in hand with simultaneously realizing a Si/high- κ layer interface of superb electrical quality—the ultimate goal of the high- κ research. Park and Ishiwara projected that the Si/LaAlO₃ structure could be a possible candidate⁵¹ as inferred from depositing the first LaAlO₃ thin films ($\kappa=20$ –27) on (100)Si using molecular beam deposition (MBD).⁵² Later, Edge *et al.* concluded through an intensive study combining Auger electron spectroscopy, infrared absorption, MEIS, HRTEM, and XPS that as-grown LaAlO₃ films on Si grown by MBD have less than 0.2 Å of SiO₂ at the LaAlO₃/Si interface.⁸ They also showed that these structures have additional favorable properties such as a 6.2 eV band gap of the LaAlO₃ layer and band offsets of 1.8 ± 0.2 eV for electrons and 3.2 ± 0.1 eV for holes.⁵³ Lu *et al.* studied amorphous LaAlO₃ films deposited on Si by laser molecular beam epitaxy in oxygen containing ambient. Here, HRTEM measurements revealed the presence of an interfacial layer, with thickness increasing with substrate temperature, introduced during film deposition.⁵⁴ The LaAlO₃ films remained amorphous after postdeposition annealing (PDA) at 1000 °C in N₂ or O₂, but were found to exhibit a better thermal stability in contact with Si when annealed in a N₂ ambient. Applying still a different deposition method, another work⁵⁵ reported on a study of LaAlO₃ films grown on Si using CVD. Also here, the analysis revealed the occurrence of an interlayer between the oxide and the Si substrate inferred as made up of compositionally graded La–Al–Si–O silicate rather than pure SiO_x. In a recent paper, Sivasubramani *et al.* reported on a study of amorphous LaAlO₃ grown on (100)Si by MBD studied as a function of postdeposition rapid thermal annealing (RTA) for 20 s in flowing N₂.¹⁰ They found the (100)Si/LaAlO₃ system to be very stable. A change in the structure of LaAlO₃

from amorphous to polycrystalline was only observed after a 935 °C RTA, followed by La and Al penetration into the Si after RTA at temperatures ≥ 950 °C. This was studied in more detail in Ref. 9.

In light of the above results, it appears of interest to get more in depth information on the true interfacial nature of Si/LaAlO₃ structures and the consequences of PDA treatments. The scope of the present work is to attain structural information on atomic scale by monitoring paramagnetic point defects in (100)Si/LaAlO₃ structures with the oxide thin films grown by MBD as a function of the PDA temperature (T_{an}). We will demonstrate, through the occurrence/absence of interface specific (P_{b0}, P_{b1}) and/or interlayer associated (*EX*) point defects, the appearance, additional growth, and modification of a SiO_x interlayer at $T_{\text{an}} > 800$ °C. At annealing temperatures up to 800 °C, the LaAlO₃/Si interface is found to be abrupt and thermally stable. A SiO_x interlayer is formed after annealing in the temperature range $T_{\text{an}} \sim 800$ –860 °C. However, this interlayer starts to break down after PDA at $T_{\text{an}} \geq 930$ °C, possibly resulting in silicate formation ($T_{\text{an}} \sim 1000$ °C).

IV. EXPERIMENTAL DETAILS

A. Sample preparation

Details about the samples studied can be found elsewhere.^{8,9,53} In short, uniform LaAlO₃ thin films (10–40 nm) were grown by MBD in an EPI 930 MBE chamber modified for the growth of oxides⁵⁶ on Si substrates. The latter were one-side polished commercial 8 in. Si wafers [*p* type, $n_a \sim (3$ – $6) \times 10^{15} \text{ B cm}^{-3}$]. Prior to deposition the native SiO₂ on the Si wafers was *in situ* thermally removed in ultrahigh vacuum at a substrate temperature of 950 °C (as measured with a pyrometer). Subsequently, using elemental sources, La, Al, and molecular oxygen (99.994%) at a background pressure of 6×10^{-8} Torr were codeposited on the substrate at ~ 100 °C. The La and Al fluxes from the effusion cells were each 2×10^{13} at./cm² s. As analyzed by Rutherford backscattering spectroscopy, this resulted in closely stoichiometric layers (La:Al molar ratio = 1 ± 0.05).

B. Electron spin resonance technique and thermal treatment

From these wafers, ESR slices of $2 \times 9 \text{ mm}^2$ main area were cut with their 9 nm edge along a $\langle 0\bar{1}1 \rangle$ direction. Cutting damage was removed through selective chemical etching of backside and edges. Thermal stability of deposited LaAlO₃ layers and interfaces was analyzed by subjecting samples to isochronal (~ 10 min) PDA at desired temperatures between 630 and 1000 °C generally in a 1 atm N₂ + 5% O₂ (99.995%) ambient or pure N₂ (99.999%) using a conventional resistively heated laboratory facility. Several sets of samples were used for the various thermal steps. As an additional test related to potential ESR activation/maximization of diamagnetic defects some samples were subjected for ~ 10 s to 10.02 eV vacuum uv photons (flux

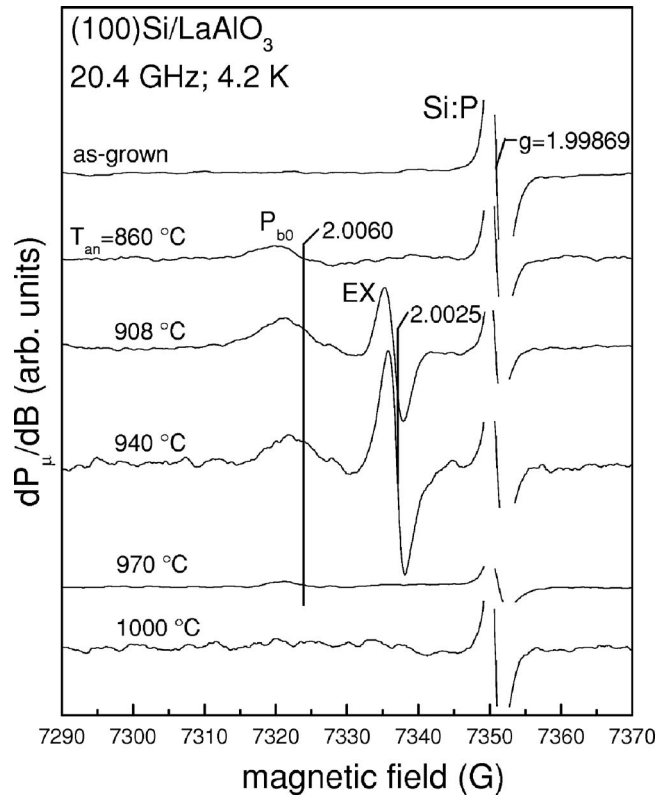


FIG. 1. Representative derivative-absorption K -band ESR spectra measured at 4.2 K with the applied magnetic field \mathbf{B} perpendicular to the interface of (100)Si/LaAlO₃ structures subjected to different steps of postdeposition annealing in N₂+5% O₂ (10 min). Spectral heights have been normalized to equal marker intensity and sample area. The applied modulation field amplitude B_m was 0.6 G and incident $P_\mu \sim 2.5$ nW. The signal at $g=1.99869$ stems from a comounted Si:P marker sample.

$\sim 5 \times 10^{14} \text{ cm}^{-2} \text{ s}^{-1}$) obtained from a Kr resonant discharge lamp or to short positive corona charging (3 μA for 10 s) in room ambient.

Conventional cw slow-passage K -band ESR measurements were carried out at 4.2 K, as described elsewhere,³³ for the applied magnetic field \mathbf{B} rotating in the (0 $\bar{1}1$) Si substrate plane over an angular range $\Phi_B=0^\circ-90^\circ$, with respect to the [100] interface normal \mathbf{n} . A comounted Si:P reference sample of $g(4.2 \text{ K})=1.99869 \pm 0.00002$ was used for g factor and spin density calibration, with the latter performed through orthodox double numerical integration of the detected derivative-absorption spectra dP_μ/dB , where P_μ is the incident microwave power. (For more details, see Ref. 33). The attained absolute and relative accuracies are estimated at $\sim 30\%$ and $\sim 10\%$, respectively. Typically, an ESR sample was comprised of 10–12 slices HF (5% in H₂O) dipped immediately before taking ESR data. Signal averaging (\sim typical 100 scans) was routinely applied to enhance spectral quality.

V. EXPERIMENTAL RESULTS AND ANALYSIS

A. Observed defects: P_{b0} and EX

Figure 1 presents an overview of representative ESR spectra, observed with $\mathbf{B} \parallel \mathbf{n}$ on the as-deposited (100)Si/LaAlO₃ structures and after different PDA steps in

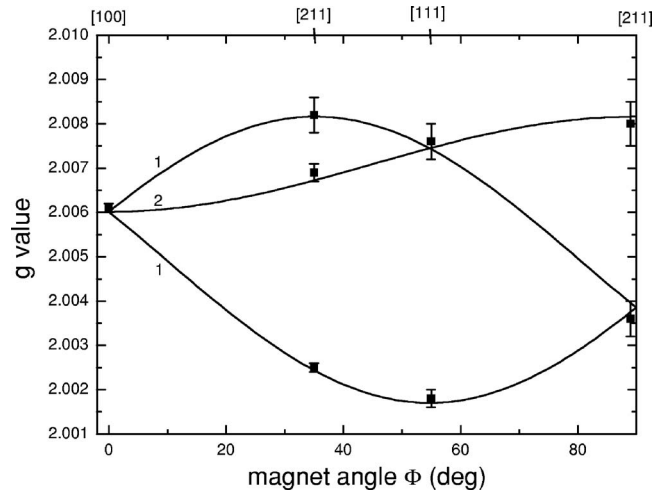


FIG. 2. Angular g map for some selected angles of the observed resonances, ascribed to P_{b0} defects for \mathbf{B} rotating in the (0 $\bar{1}1$) plane with respect to the interface normal \mathbf{n} observed in a (100)Si/LaAlO₃ structure subjected to a postdeposition annealing at 900 °C for ~ 10 min. The curves represent the optimized fitting of the various branches for axial symmetry yielding $g_{\parallel}=2.0017 \pm 0.0001$ and $g_{\perp}=2.0082 \pm 0.0001$, found within experimental accuracy to be in agreement with the P_{b0} data for standard thin thermal oxide/Si structures, affirming the P_{b0} assignment. The added numbers indicate relative branch intensities expected from the standard defect model, also matching experimental observation.

N₂+5% O₂ ambient. Within spectral accuracy, no ESR active defects could be observed on the as-grown samples, the situation remaining unaltered for annealing up to $T_{\text{an}} \leq 800$ °C. However, upon annealing in the temperature range $T_{\text{an}} \sim 860$ –970 °C, a resonance signal is observed at zero crossing $g=2.0060 \pm 0.0001$ with $\Delta B_{\text{p.p.}}=7 \pm 1$ G, exhibiting distinct angular anisotropy. To trace the signal's origin, a coarse g map was composed for \mathbf{B} rotating in the (0 $\bar{1}1$) plane. As shown in Fig. 2, the obtained data could be well fitted by an axial symmetric system (see solid curves in Fig. 2) with principal g values $g_{\parallel}=2.0017 \pm 0.0001$ and $g_{\perp}=2.0082 \pm 0.0001$. These results match those obtained for the g pattern of the P_{b0} defect in standard thin Si/SiO₂ systems,³⁶ leaving little doubt about the signal's origin. It appears that the (100)Si/LaAlO₃ interface has become Si/SiO₂-type, evidencing that a SiO_x-type interlayer has formed. For completeness, with respect to the results for the $T_{\text{an}} \leq 800$ °C range where no ESR signal could be detected, this would indicate, if drawing on the estimated detection limit for an interface defect such as P_{b0} over reasonable averaging times, any occurring density to be below $\sim 4 \times 10^{10} \text{ cm}^{-2}$.

Here, we should add that some of the PDA steps at representative temperatures were also carried out in pure (99.999%) N₂. Generally, these led to similar ESR results as those for the O₂/N₂ ambient, with no outspoken effect on P_{b0} appearance. So, while it cannot entirely be excluded that the presence of O₂ in the annealing ambient might have promoted the Si/SiO_x interface formation, its effect is not conclusive.

As can be seen from Fig. 1, one more signal is observed after annealing in the range $T_{\text{an}} \sim 888$ –940 °C at $g=2.0025 \pm 0.0001$. It could be conclusively identified as the

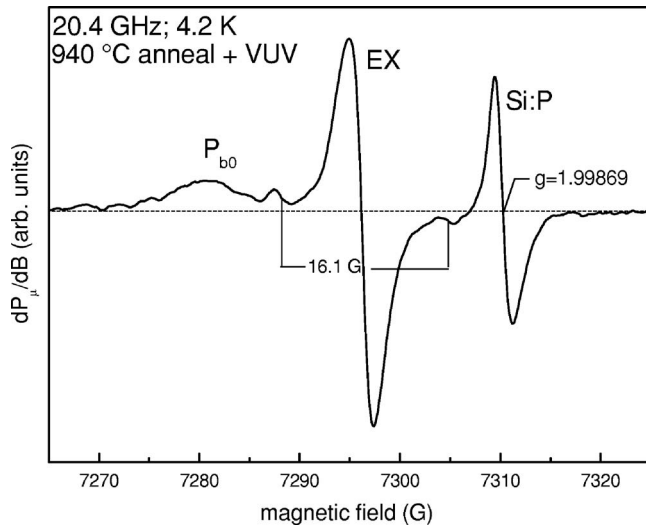


FIG. 3. Derivative-absorption K -band ESR spectrum improved through signal averaging (~ 200 scans) of the observed defects measured at 4.2 K on (100)Si/LaAlO₃ subjected to postdeposition annealing in N₂+5% O₂ (10 min) at 940 °C and additional vuv irradiation.

EX signal from the observed accompanying hyperfine doublet (16.1 G splitting) centered around this g value, typical for this defect. This is evident from Fig. 3 showing a zoomed-in representative spectrum of the EX center observed in the sample subjected to a 940 °C annealing and additional vuv irradiation. As outlined above, the EX defect is a SiO₂ associated center, well known from studies of bulk SiO₂ and various kinds of Si/SiO₂ structures.^{16,38–48}

In the as-deposited and PDA treated samples, no LaAlO₃-specific point defects could be observed. Quite surely, though, point defect sites will be present, but reside in a diamagnetic state, making them invisible for ESR detection. So to probe deeper it was aimed to maximally reveal defects in the oxide as well as at the interface, through subjecting some samples to additional vuv irradiation—known to be an efficient means for both oxide^{57–59} and interface defects in Si/SiO₂ to photodissociate H-terminated dangling bonds and to possibly additionally unveil weak or strained bonds.^{60,61} Still any evidence for LaAlO₃-associated defects remained lacking as no ESR spectral changes were noticed.

Importantly as one more result, this finding thus also indicates that no P_b -type defect system remained hidden or was left partially passivated—as could be expected from the H-free fabrication process of the samples. In the same spirit, some samples were additionally subjected to positive corona charging, applied for a very short time (10 s) though to avoid impairing H-related effects inherent to such method,⁶² to possibly put diamagnetic defects in the LaAlO₃ in the correct charge state for ESR detection. Yet, in spite of these efforts, detection of any LaAlO₃-related defects still failed.

B. Defect densities versus T_{an}

Monitoring the defect densities of the observed defects, P_{b0} and EX , as a function of PDA treatment revealed various interesting aspects about the nature and stability of the (100)Si/LaAlO₃ interface. The main PDA results (5% O₂

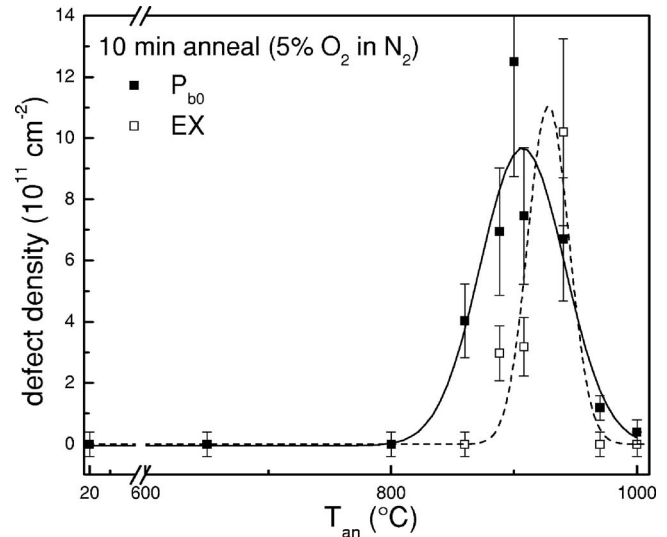


FIG. 4. Compilation of the inferred defect densities in (100)Si/LaAlO₃ entities as a function of the postdeposition isochronal annealing in N₂+5% O₂ (10 min) for P_{b0} and EX centers, represented by closed and open symbols, respectively. The solid and dashed traces are Gaussian curves, merely meant to guide the eye in exposing the peaking in defect generation and the somewhat lagging behind (~ 30 °C) of EX production vis-à-vis P_{b0} appearance. Data points at zero defect density symbolize failure of signal detection.

+N₂) are compiled in Fig. 4, showing the density of observed defects as a function of PDA temperature. Various items are worth noting.

No ESR signals, in particular, no P_b -type defects could be observed in the as-deposited Si/LaAlO₃ structure. On the basis of the latter criterion it evidences, with atomic level sensitivity, that there is no SiO_x-type interlayer present or that this interlayer is at least substantially thinner than⁶³ 3 Å—an abrupt interface—which is in good agreement with our previous results.⁸ This is in sharp contrast with other stacks of (100) Si with high- κ layers, such as Al₂O₃, HfO₂, and ZrO₂, where the presence of such an interlayer appeared inevitable, even in the as-deposited state, which was revealed by ESR.^{14–19} The abrupt interface remains unaltered even during subsequent annealing up to $T_{an} \sim 800$ °C, indicating that the interface is thermally stable.

After annealing at $T_{an} \sim 860$ °C a SiO_x-type interlayer has formed, as evidenced by the observation of P_{b0} defects. Upon annealing at a slightly higher temperature $T_{an} \sim 888$ °C, the SiO₂-associated EX defect appears, so, delayed over ~ 30 °C in terms of T_{an} . This observation corroborates the presence of a SiO_x-type interlayer and also indicates an additional growth of the interlayer. The defect was not observed in the sample annealed at $T_{an} \sim 860$ °C even though the presence of a SiO_x-type interlayer in this sample is signaled by the observation of P_{b0} defects. It suggests that a minimal thickness of the SiO_x interlayer is needed for (ESR) detectable formation of EX defects, at least more substantial than required for effective Si/SiO_x-interface formation. The need of a minimal thickness of SiO₂ for EX detection has been reported before for dry thermal SiO₂ on Si.³⁹ Thus the retardation in EX appearance vis-à-vis P_{b0} would indicate an additional growth (or modification) of the interlayer. The interlayer thickness, however, is unknown. In

broader context, it is interesting to note that the generation of *EX* centers upon annealing at elevated temperatures in oxygen-containing ambients appears symptomatic for stacks of high- κ metal oxide layers on Si.¹⁶

VI. DISCUSSION

A. Interlayer formation and disintegration

Monitoring of occurring point defects as a function of PDA treatment, additional vuv irradiation, and corona charging revealed interesting information on the annealing induced structural/compositional changes in the interface region. Compiling the thermal evolution of the observed defect densities, hereby displaying all main results, Fig. 4 will guide the discussion and interpretation. Prominently, the defect density versus T_{an} curves show a peaked behavior, simulated by Gaussian curves. The maximum P_{b0} density, $[P_{b0}] \sim (1.3 \pm 0.3) \times 10^{12} \text{ cm}^{-2}$, is obtained at $T_{\text{an}} = 900 \text{ }^\circ\text{C}$ while the maximum *EX* density, $[EX] \sim (1.0 \pm 0.3) \times 10^{12} \text{ cm}^{-2}$, is obtained at a slightly higher PDA temperature $T_{\text{an}} = 940 \text{ }^\circ\text{C}$. On the account of P_{b0} , it appears that for annealing from $T_{\text{an}} > 900 \text{ }^\circ\text{C}$ onward, the interface starts to break up first, where it is interesting to note that, in the range $T_{\text{an}} \sim 900\text{--}940 \text{ }^\circ\text{C}$, the *EX* density still increases while the P_{b0} density already starts to decrease. So, the overall picture emerging from the curves in Fig. 4 is that, as compared to P_{b0} , the manifestation of the *EX* peak is delayed in terms of T_{an} . The true character of the Si/SiO_x-type interface is disrupted first (elimination of interfacial Si dangling bonds), but for $T_{\text{an}} \geq 940 \text{ }^\circ\text{C}$, the defects rapidly disappear altogether, pointing to drastic disintegration of the interfacial region, i.e., elimination of the “pure” SiO_x component. For clarity, this disappearance of the ESR-active centers is not due to inadvertent H passivation, as verified by applying additional vuv irradiation after some PDA steps. The structural/chemical change breaking up the interlayer seems to first affect the P_{b0} defects located at the interface before it affects the interlayer associated *EX* defects.

B. Influence of oxide crystallization and interdiffusion

It is interesting to put the currently acquired atomic level information in terms of occurring point defects in the perspective of previous morphological/compositional studies^{8,10,52,54} on the Si/LaAlO₃ structure. Using such methods, recent work¹⁰ has investigated the thermal stability of (100)Si/LaAlO₃/Al₂O₃ stacks against RTA in N₂ ambient at 850–1040 °C for 10–20 s. As observed by atomic force microscopy and x-ray diffraction, the work reports that RTA from 900 °C onward starts to induce changes in surface morphology, together with initiation of the transformation of the amorphous to a polycrystalline state, in agreement with previous results on LaAlO₃ films produced by different methods. Secondary ion mass spectroscopy (SIMS) profiling shows that substantial penetration of Al and La atoms into the Si substrate occurs for RTA at or above 950 °C, with in fact any penetration effects remaining below the detection limit for $T_{\text{an}} \leq 935 \text{ }^\circ\text{C}$.

Our ESR data may well fit within this morphological picture: In terms of T_{an} , we may link the initiation of the

formation of a Si/SiO_x-type interface with the very early onset of LaAlO₃ film crystallization, followed by some more substantial SiO_x-type interlayer growth with increasing T_{an} . For clarity, though, the appearance of the P_{b0} centers cannot be directly linked to the grain boundary regions per se, as this would conflict with the observed ESR spectral anisotropy in registry with the crystalline (100) Si surface. Then, for T_{an} further increasing above $\sim 940 \text{ }^\circ\text{C}$, the progressing interdiffusion chemically destroys the pristine nature of the SiO_x component (possibly silicate formation) resulting in the obliteration of the SiO_{2(x)}-specific point defects. It is possible that the onset temperature for La and Al outdiffusion in the current case is somewhat lower considering the applied longer PDA treatment times (10 min) as compared to previous RTA work (10–20 s).

Also, within the interpretation, it appears that we detect the initiation of crystallization of the amorphous LaAlO₃ film somewhat at lower T_{an} than in previous work.¹⁰ Again, this may partly have resulted from the applied longer annealing times in conjunction with the presence of O₂ in the annealing ambient. Yet, it may as well bear out the fact that ESR is prone to detect interfacial reshaping in a very embryonic state, ahead of standard morphological /compositional methods.

C. Absence of P_{b1} defect

The observation of the P_{b0} defect indicates that a Si/SiO₂-type interface has formed. As demonstrated, the obtained ESR parameters such as *g* value, linewidth, and defect density are indeed very similar to those characteristic for thermal Si/SiO₂ interfaces. There is, however, one remarkable apparent dissonance: No P_{b1} ($g_1 = 2.00577$, $g_2 = 2.00735$, $g_3 = 2.0022$) centers could be detected. As outlined, the P_{b1} center also concerns an unpaired *sp*³ hybrid at a threefold Si atom part of a strained Si–Si dimer ($\equiv\text{Si}-\text{Si}'=\text{Si}_2$), thus basically chemically identical to the P_{b0} center, yet physically different, e.g., regarding hybrid orientation, bond strain, and structural relaxation.³⁴ Generally, the P_{b0} and P_{b1} centers are almost invariably observed in tandem at the (100)Si/SiO₂ interface, although relative intensities may vary. So, the question arises as to the absence of the P_{b1} defect, at least below ESR sensitivity, at the current Si/SiO_{2(x)}-type interface formed during PDA of (100)Si/LaAlO₃ entities. There may be several reasons. One considered here concerns interfacial strain. Pertinently, the P_{b1} center may be less prominent, even absent beyond the detection limit in Si/SiO₂ entities grown at low T_{ox} or after particular PDAs. In previous work,⁶⁴ it has been outlined that this would not just be the result of the small oxide thickness per se, as compared to more standard SiO₂ thicknesses ($\geq 10 \text{ nm}$). Rather, P_{b1} formation would require a minimum amount of oxide (interface) relaxation as generally inherently established during oxidation at high T_{ox} . So, as a possibility, sufficient interface relieve may not have been attained in the current case, not even for PDA steps up to 950 °C. Possibly, in this the top LaAlO₃ layer plays a constraining role.

VII. CONCLUSIONS

The ESR technique has been successfully applied to assess the nature of the interface in (100)Si/LaAlO₃ entities and thermally induced alterations. It is found that the (100)Si/LaAlO₃ structure exhibits a high quality and robust interface in terms of DB-type interface defects, stable under extended thermal annealings up to ~850 °C, even in O₂-containing ambient.

Upon annealing at $T_{\text{an}} \geq 860$ °C a SiO_x-type interlayer is formed as evidenced by the appearance of P_{b0} interface defects, an effect likely forerunning or heralding the onset of crystallization of the *a*-LaAlO₃ film. At somewhat higher annealing temperature, the EX defect is observed, the delay in appearance vis-à-vis P_{b0} pointing to additional growth of the SiO_x-type interlayer. However, upon annealing at temperatures $T_{\text{an}} \geq 930$ °C, the Si/SiO_x nature of the interlayer starts to break up again, resulting in fast, likely compositional, transformation with increasing T_{an} as signaled by the disappearance of the SiO_x-related defects altogether. It is ascribed to invasive diffusion of La and Al into the Si substrate, possibly resulting in silicate (interlayer) formation.

Generally, ESR has emerged as a viable technique to trace thermally induced structural/compositional alterations in Si/insulator entities through probing the incorporation of interface-/interlayer-related point defects. The method takes a separate position in the sense that it may reveal such changes on atomic level where standard morphological/structural analyzing tools simply fall short, or detect these at an earlier stage before the latter may achieve.

- ¹G. D. Wilk, R. M. Wallace, and J. M. Anthony, *J. Appl. Phys.* **89**, 5243 (2001).
²M. Houssa *et al.*, *Mater. Sci. Eng.*, **R** **51**, 37 (2006).
³See the *International Technology Roadmap for Semiconductors*, 2005 ed. (Semiconductor Industry Association, San Jose, CA, 2005).
⁴M. A. Quevedo-Lopez, M. El-Bouanani, B. E. Gnade, R. M. Wallace, M. R. Visokay, M. Douglas, M. J. Bevan, and L. Colombo, *J. Appl. Phys.* **92**, 3540 (2002).
⁵J. Robertson, *Eur. Phys. J.: Appl. Phys.* **28**, 265 (2004).
⁶See, e.g., W. Vandervorst *et al.*, *Mater. Res. Soc. Symp. Proc.* **745**, 23 (2003).
⁷G. A. Botton, E. Romain, D. Landheer, X. Wu, M.-Y. Wu, M. Lee, and Z.-H. Lu, *Proc.-Electrochem. Soc.* **2003-02**, 251 (2003).
⁸L. F. Edge *et al.*, *Appl. Phys. Lett.* **84**, 4629 (2004).
⁹L. F. Edge *et al.*, *Appl. Phys. Lett.* **89**, 062902 (2006).
¹⁰P. Sivasubramani, M. J. Kim, B. E. Gnade, R. M. Wallace, L. F. Edge, D. L. Schlom, H. S. Craft, and J. P. Maria, *Appl. Phys. Lett.* **86**, 201901 (2005).
¹¹B. H. Lee, L. Kang, R. Nieh, W. J. Qi, and J. C. Lee, *Appl. Phys. Lett.* **76**, 1926 (2000).
¹²M. Copel, M. Gribelyuk, and E. Gusev, *Appl. Phys. Lett.* **76**, 436 (2000); C. M. Perkins, B. B. Triplett, P. C. McIntyre, K. C. Saraswat, S. Haukka, and M. Tuominen, *ibid.* **78**, 2357 (2001); M. Gutowski, J. E. Jaffe, C.-L. Liu, M. Stoker, R. I. Hedge, R. S. Rai, and P. J. Tobin, *ibid.* **80**, 1897 (2002).
¹³M. Cho, J. Park, H. B. Park, C. S. Hwang, J. Jeong, and K. S. Hyun, *Appl. Phys. Lett.* **81**, 334 (2002); M. R. Visokay, J. J. Chambers, A. L. Rondardo, A. Shanware, and L. Colombo, *ibid.* **80**, 3183 (2002).
¹⁴A. Stesmans and V. V. Afanas'ev, *J. Phys.: Condens. Matter* **13**, L673 (2001); *Appl. Phys. Lett.* **80**, 1957 (2002).
¹⁵A. Y. Kang, P. M. Lenahan, J. F. Conley, Jr., and R. Solanski, *Appl. Phys. Lett.* **81**, 1128 (2002).
¹⁶A. Stesmans and V. V. Afanas'ev, *J. Appl. Phys.* **97**, 033510 (2004).
¹⁷J. L. Cantin and H. J. von Bardeleben, *J. Non-Cryst. Solids* **303**, 175 (2002).

- ¹⁸S. Baldovino, S. Nokrin, G. Scarel, M. Fanciulli, T. Graf, and M. S. Brandt, *J. Non-Cryst. Solids* **322**, 168 (2003).
¹⁹B. J. Jones and R. C. Barklie, *Microelectron. Eng.* **80**, 74 (2005).
²⁰M. Houssa, A. Stesmans, M. Naili, and M. M. Heyns, *Appl. Phys. Lett.* **77**, 1381 (2000).
²¹J. R. Chavez, R. A. B. Devine, and L. Koltunski, *J. Appl. Phys.* **90**, 4284 (2001).
²²V. V. Afanas'ev and A. Stesmans, *Appl. Phys. Lett.* **80**, 1261 (2002).
²³R. J. Carter *et al.*, *International Workshop on Gate Insulators*, edited by S. Ohmi, F. Fujita, and H. S. Momose (Japan Society of Applied Physics, Tokyo, 2001), p. 94.
²⁴X. Garros, G. Reimbold, D. Duret, C. Leroux, B. Guillaumot, O. Louveau, C. Hobbs, and F. Martin, *Proceedings 43rd Annual IEEE International Reliability Physics Symposium*, 2005 (unpublished).
²⁵P. Masson, J. L. Autran, M. Houssa, X. Garros, and C. Leroux, *Appl. Phys. Lett.* **81**, 3392 (2002).
²⁶B. J. O'Sullivan *et al.*, *J. Electrochem. Soc.* **151**, 493 (2004).
²⁷R. J. Carter, E. Cartier, A. Kerber, L. Pantisano, T. Schram, S. De Gendt, and M. Heyns, *Appl. Phys. Lett.* **83**, 533 (2003).
²⁸M. Schmidt, M. C. Lemme, H. Kurz, T. Witters, T. Schram, K. Cherkaoui, A. Negara, and P. K. Hurley, *Microelectron. Eng.* **80**, 70 (2005).
²⁹M. Copel and M. C. Reuter, *Appl. Phys. Lett.* **83**, 3398 (2003).
³⁰A. Stesmans and V. V. Afanas'ev, *Phys. Rev. B* **57**, 10030 (1998).
³¹R. Helms and E. H. Poindexter, *Rep. Prog. Phys.* **57**, 791 (1994).
³²K. Brower, *Phys. Rev. B* **33**, 4471 (1986); *Appl. Phys. Lett.* **43**, 1111 (1983).
³³A. Stesmans, *Phys. Rev. B* **48**, 2418 (1993).
³⁴A. Stesmans, B. Nouwen, and V. V. Afanas'ev, *Phys. Rev. B* **58**, 15801 (1998).
³⁵E. H. Poindexter and P. J. Caplan, in *Insulating Films on Semiconductors*, edited by M. Schultz and G. Pensl (Springer, Berlin, 1981), p. 150.
³⁶A. Stesmans and V. V. Afanas'ev, *J. Appl. Phys.* **83**, 2449 (1998).
³⁷W. Futako, M. Mizuochi, and S. Yamasaki, *Phys. Rev. Lett.* **92**, 105505 (2004).
³⁸A. Stesmans, *Phys. Rev. B* **45**, 9502 (1992).
³⁹A. Stesmans and F. Scheerlinck, *J. Appl. Phys.* **75**, 1047 (1994).
⁴⁰A. Stesmans and F. Scheerlinck, *Phys. Rev. B* **50**, 5204 (1994).
⁴¹W. E. Carlos and S. M. Prokes, *J. Appl. Phys.* **78**, 2129 (1995).
⁴²H. J. von Bardeleben, C. Ortega, A. Grosman, V. Morazzani, J. Siejka, and D. Stievenard, *J. Lumin.* **57**, 301 (1993).
⁴³A. Stesmans, B. Nouwen, and V. V. Afanas'ev, *Phys. Rev. B* **66**, 045307 (2002).
⁴⁴A. Baumer, M. Stutzmann, M. S. Brandt, F. C. K. Au, and T. S. Lee, *Appl. Phys. Lett.* **85**, 943 (2004).
⁴⁵R. P. Wang, *Appl. Phys. Lett.* **88**, 142104 (2006).
⁴⁶M. Dohi, H. Yamatani, and T. Fujita, *J. Appl. Phys.* **91**, 815 (2002).
⁴⁷A. Stesmans, K. Clémer, and V. V. Afanas'ev, *Phys. Rev. B* **72**, 155335 (2005).
⁴⁸H. J. von Bardeleben, J. L. Cantin, J. J. Ganem, and I. Trimaille, in *Defects in High-κ Gate Dielectric Stacks*, NATO Science Series, edited by E. Gusev (Kluwer, Dordrecht, 2006), p. 263.
⁴⁹B. B. Triplett, P. T. Chen, Y. Nishi, P. H. Kasai, J. J. Chambers, and L. Colombo, *J. Appl. Phys.* **101**, 013703 (2007).
⁵⁰H. Kusumoto and M. Shoji, *J. Phys. Soc. Jpn.* **17**, 1678 (1962).
⁵¹B. E. Park and H. Ishiwara, *Appl. Phys. Lett.* **79**, 806 (2001).
⁵²B. E. Park and H. Ishiwara, *Appl. Phys. Lett.* **82**, 1197 (2003).
⁵³L. F. Edge, D. G. Schlom, S. A. Chambers, E. Cicerrella, J. L. Freeouf, B. Holländer, and J. Schubert, *Appl. Phys. Lett.* **84**, 726 (2004).
⁵⁴X. B. Lu *et al.*, *Appl. Phys. Lett.* **84**, 2620 (2004).
⁵⁵Q. Y. Shao, *Appl. Phys. A: Mater. Sci. Process.* **81**, 1181 (2005).
⁵⁶J. Lettieri, J. H. Haeni, and D. G. Schlom, *J. Vac. Sci. Technol. A* **20**, 1332 (2002).
⁵⁷J. I. Pankev, D. E. Carlson, J. E. Berkeyheiser, and R. O. Wance, *Phys. Rev. Lett.* **51**, 2224 (1983).
⁵⁸D. L. Griscom, *J. Appl. Phys.* **58**, 2524 (1985), and references therein.
⁵⁹A. H. Edwards, *J. Non-Cryst. Solids* **187**, 232 (1995).
⁶⁰A. Pusel, U. Wetterauer, and P. Hess, *Phys. Rev. Lett.* **81**, 645 (1998).
⁶¹T. Vondrak and X. Y. Zhu, *J. Phys. Chem. B* **103**, 4892 (1999).
⁶²A. Stesmans and V. V. Afanas'ev, *Appl. Phys. Lett.* **82**, 2835 (2003).
⁶³W. Futako, T. Umeda, M. Nishizawa, T. Yasuda, J. Isoya, and S. Yamasaki, *J. Non-Cryst. Solids* **299-302**, 575 (2002); *Phys. Rev. Lett.* **92**, 105505 (2004).
⁶⁴A. Stesmans and V. V. Afanas'ev, *Appl. Phys. Lett.* **77**, 1469 (2000).

Journal of Applied Physics is copyrighted by the American Institute of Physics (AIP).
Redistribution of journal material is subject to the AIP online journal license and/or AIP
copyright. For more information, see <http://ojps.aip.org/japo/japcr/jsp>